



available at www.sciencedirect.com

SCIENCE @ DIRECT®

ELSEVIER

journal homepage: www.elsevier.com/locate/jhydrol



A reservoir operation scheme for global river routing models

Naota Hanasaki *, Shinjiro Kanae, Taikan Oki

Institute of Industrial Science, University of Tokyo, Be607, 4-6-1 Komaba, Meguro-ku, Tokyo 153-8505, Japan

Received 6 August 2004; received in revised form 10 October 2005; accepted 10 November 2005

KEYWORDS

Dams;
Fluvial hydrology;
Global model;
Irrigation;
Reservoir effects

Summary A global river discharge simulation was conducted that accounted for 452 individually operated reservoirs by locating them on the digital global river network map of TRIP, a global river routing model. An operating rule was determined for each reservoir using a newly-developed algorithm that used currently available global data such as reservoir storage capacity, intended purposes, simulated inflow, and water demand in the lower reaches. This algorithm reduced the root mean square error of reservoir release and river discharge simulations from that of earlier global river discharge simulations that neglected reservoir operations or substituted an algorithm for natural-lake outflow. The 2-year global simulation results indicate that reservoir operations substantially altered monthly discharge for individual basins (i.e., by more than 20%). Averaged over the continental scale, the maximum change in monthly river discharge varied from 0% to 34% and the changes in reservoir storage were small as a proportion of the total storage capacity.

© 2005 Elsevier B.V. All rights reserved.

Introduction

More than 45,000 large dams have been constructed globally (WCD, 2000), with a total storage capacity of 7000 km³ (ICOLD, 1998). This large volume of water amounts to three times the annual average water storage in river channels (1200–2120 km³), or one-sixth of the global annual river

discharge (40,000 km³ yr⁻¹; Baumgartner and Reichel, 1975). Taking these numbers at face value, reservoir operations would seem to have considerable potential impact on the terrestrial water cycle. This raises questions about how large reservoir operations alter river flow; how much water, and at what times, is stored behind dams; and the extent to which reservoir operations alter the terrestrial water cycle. Our study examines one aspect of how human activity changes the global environment.

Several earlier studies of anthropogenic impacts on the global water cycle have been reported. Nilsson and colleagues assessed anthropogenic impacts on rivers in the northern third of the world (Mexico, United States, Canada, Europe, and countries of the former Soviet Union) and over

* Corresponding author. Tel.: +81 3 5452 6382; fax: +81 3 5452 6383.

E-mail addresses: hanasaki@iis.u-tokyo.ac.jp (N. Hanasaki), kanae@iis.u-tokyo.ac.jp (S. Kanae), taikan@iis.u-tokyo.ac.jp (T. Oki).

the entire globe (Dynesius and Nilsson, 1994; Nilsson et al., 2005). They developed an index of flow regulation for major rivers, taking into account reservoir operation, inter-basin water transfer, and irrigation consumption. For reservoir operation, they calculated the ratio of reservoir capacity to mean annual inflow for each basin. Vörösmarty et al. (1997) assessed the storage and residence time of continental runoff in large reservoirs around the world. They located 622 reservoirs with more than $500 \times 10^6 \text{ m}^3$ of storage capacity on their global digital river network map and discussed river water residence times by examining storage capacity and mean annual inflow for each reservoir and basin. These studies used the ratio of mean annual inflow to storage capacity as an index of the potential impact of reservoir operation. This index, however, ignores seasonal variation in the re-allocation of river flow, the most basic function of reservoirs, as well as the magnitude of the storage volume that is carried over between years.

One option to quantify the impact of reservoir operation on river flow at the global scale is to use a global river routing model (see Miller and Russell, 1990; Oki et al., 1999; Fekete et al., 2000). These models consist of a digital global river network map that delineates the major rivers and calculates the discharge at each grid point. The problem is how to incorporate reservoir operations into these models.

Several studies have incorporated reservoir operation into large-scale hydrological models. For example, Meigh et al. (1999) estimated water scarcity for eastern and southern Africa using a grid-based model and incorporated reservoir outflows as outflow regulation, storage, and run-of-the-river reservoirs using the following assumptions. For outflow regulation reservoirs, outflow (Q_{out}) was proportional to the current storage (S_i) raised to a power of 1.5 ($Q_{\text{out}} = S_i^{1.5}$). For water storage reservoirs, any water released was used to meet demands and once the reservoir was filled, the outflow equaled the amount spilled. Run-of-the-river reservoirs had little impact on downstream flows. Coe (2000) developed a global hydrological routing algorithm (HYDRA) for reservoir operations on the Paraná River. He summed the maximum storage capacity and surface area of reservoirs upstream of Guaira, Brazil, and treated them as a single reservoir. Storage was set at maximum capacity when the mean monthly flux into the basin was greatest, and at minimum capacity (10% of the maximum) when the inflow was lowest. Döll et al. (2003) conducted a global river discharge simulation accounting for reservoir flow regulation. They modified the model of Meigh et al. (1999) and parameterized reservoir release as:

$$Q_{\text{out}} = k_r \times S_r \left(\frac{S_r}{S_{r\max}} \right)^{1.5}, \quad (1)$$

where Q_{out} is outflow ($\text{m}^3 \text{ d}^{-1}$), k_r is an outflow coefficient (0.01 d^{-1}), and S_r is actual active storage (m^3), $S_{r\max}$ is maximum active storage capacity ($S_r \leq S_{r\max}$). They assumed that $S_{r\max} = A_{\text{lake}} H$, where A_{lake} is the surface area of the storage lake (m^2) and H is the maximum active storage depth (fixed at 5 m, globally). This parameterization was developed for global lakes, but was also applied to reservoirs because of a lack of information on their management. Areas of lakes were obtained from the Global Lakes and Wetlands Database (GLWD; Lehner and Döll, 2004). Hadde-land et al. (in press) assessed the effect of irrigation on the

water and energy balances of the Colorado and Mekong River basins and incorporated reservoir operations. They set operating rules using hydropower and irrigation water demand and historical flow data. In periods of water scarcity, they assumed that irrigation water was extracted from reservoirs.

To incorporate reservoir operations in global river routing models, global applicability is an important concern. Meigh et al. (1999), Coe (2000) and Haddeland et al. (in press) set reservoir operation rules individually, taking actual operations into account. This is a reliable approach; however, reservoir operating records are not always published, especially in developing countries, and it is impractical to collect these data for the entire world. In contrast, Nilsson et al. (2005), Vörösmarty et al. (1997) produced comprehensive global analyses of reservoirs, although they did not develop or use global models that incorporated individual reservoir operations. The parameterization of Döll et al. (2003) is globally applicable because it only requires surface areas, which are globally available for large reservoirs (Lehner and Döll, 2004).

We developed a new algorithm for setting operating rules for individual reservoirs in global river routing models. We considered that actual operating rules are set using the specifications of each reservoir, the hydrometeorological conditions of the basin, and the water demand in the lower reaches. We designed the algorithm for use with currently available global data such as existing global reservoir datasets, global river discharge simulation results, and global water use information. Following Vörösmarty et al. (1997), we placed major reservoirs at grid points on a digital map of the global river routing network model, and set operating rules for each reservoir. Thus, a global river discharge simulation was conducted accounting for 452 individually operated reservoirs. The algorithm did not exactly reproduce actual reservoir operations because of a lack of detailed information; however, it improved the reservoir outflow and global river discharge simulation compared to previous studies. Finally, the quantitative impact of reservoir operation on the terrestrial water cycle was discussed.

Data

Reservoir data

Reservoir information was obtained from the World Register of Dams 1998 (WRD98; ICOLD, 1998). In all, 593 reservoirs with more than $1000 \times 10^6 \text{ m}^3$ of storage capacity were selected. Data for each dam or reservoir, such as name, year of construction, storage capacity, catchment area, and purposes (in order of importance), were compiled electronically. Geographical locations (longitude/latitude) were obtained from Vörösmarty et al. (1997), Lehner and Döll (2004), and a world atlas (Shobunsha, 2000) because WRD98 provides only the name of the river and the nearest city, province, and country as location information. We obtained the locations of 498 reservoirs and placed them on the digital river network map of the Total Runoff Integrating Pathways model (TRIP; Oki and Sud, 1998; see Fig. 1) which has a spatial resolution of 1° longitude \times 1° latitude. Ninety-five reservoirs could not be located, and 46 reservoirs that

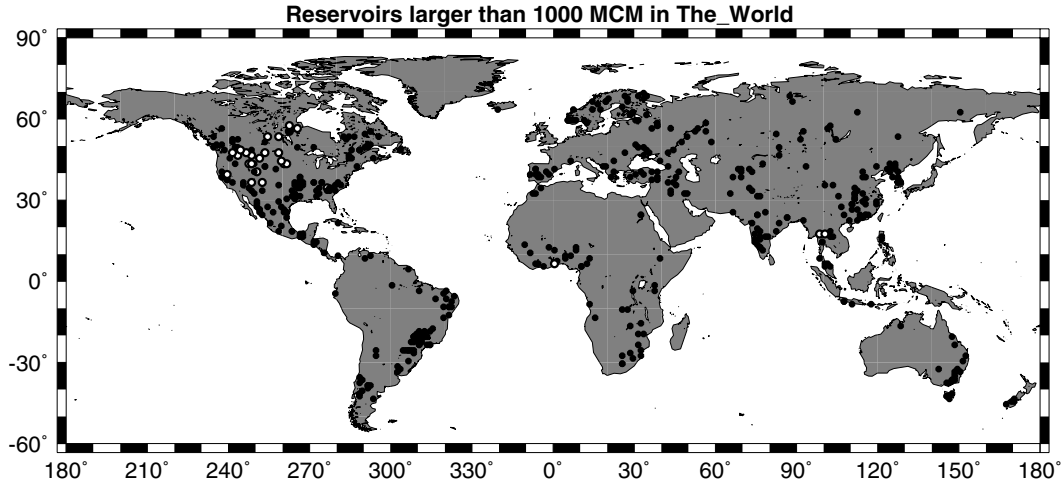


Figure 1 Global distribution of reservoirs with greater than $1000 \times 10^6 \text{ m}^3$ storage capacity. Open circle: validation sites.

were constructed after 1987 were removed because the simulation period was for 1987–1988. The total storage capacity of the 452 reservoirs was 4140 km^3 or about 60% of the total storage capacity of all the large reservoirs in the world (7000 km^3).

To check whether the located reservoirs adequately covered the range of hydrological characteristics, catchment areas calculated from the TRIP digital river map were compared with those published for 69 reservoirs in the United States (Fig. 2). Catchment areas were generally overestimated on the TRIP map, and were more accurate for reservoirs larger than $50,000 \text{ km}^2$. The spatial resolution of this map was $1^\circ \times 1^\circ$ and gave an area of approximately $12,000 \text{ km}^2$ at the equator; this represented the minimum catchment area. Thus, the error is high if catchment areas

are smaller than this minimum; on a global river map with a finer spatial resolution, this error would be reduced. The overestimation of catchment area leads to overestimation of inflow to reservoirs; this effect is discussed in "Sensitivity test".

Global river discharge data

For the baseline global river discharge simulation, we referred to Oki et al. (1999) who used TRIP and routed the gridded global runoff field provided by the Global Soil Wetness Project (GSWP; Dirmeyer et al., 1999). The GSWP is ongoing environmental modeling research, with a goal of producing state-of-the-art global datasets for land surface fluxes, state variables, and related hydrological quantities. The datasets, including runoff fields, are produced by integrating uncoupled land surface models (LSMs) using near-surface meteorological data provided by the International Satellite Land-Surface Climatology Project (ISLSCP, Meeson et al., 1995) and standardized soil and vegetation parameters provided by GSWP. Both the runoff field and the digital river network map have $1^\circ \times 1^\circ$ (longitude, latitude) spatial resolution. The runoff field has 10-day temporal resolution for 2 years (1987–1988). Oki et al. (1999) averaged the output of 11 participating LSMs of GSWP to reduce the model bias; however, this also reduced temporal fluctuations in the runoff. In this study, we used only results from the SiB model (Sellers et al., 1986) operated by the Japan Meteorological Agency (hereafter, JMA-SiB). We selected JMA-SiB because its global distribution of annual runoff is closest to the mean of 11 LSMs (the number of grid squares with more than 10% difference was smallest among these 11 LSMs). Using the global runoff field of JMA-SiB, global river discharge simulation (hereafter, no-reservoir simulation) was conducted.

Oki et al. (1999) reported a limitation of the global river discharge simulation using GSWP runoff. They noted that while the GSWP runoff dataset reproduced seasonal patterns of river discharge well, it underestimated annual total river discharge. The simulated global annual total river discharge for the average of the 11 GSWP-participating LSMs was $28,845 \text{ km}^3 \text{ yr}^{-1}$ ($30,519 \text{ km}^3 \text{ yr}^{-1}$ using JMA-SiB),

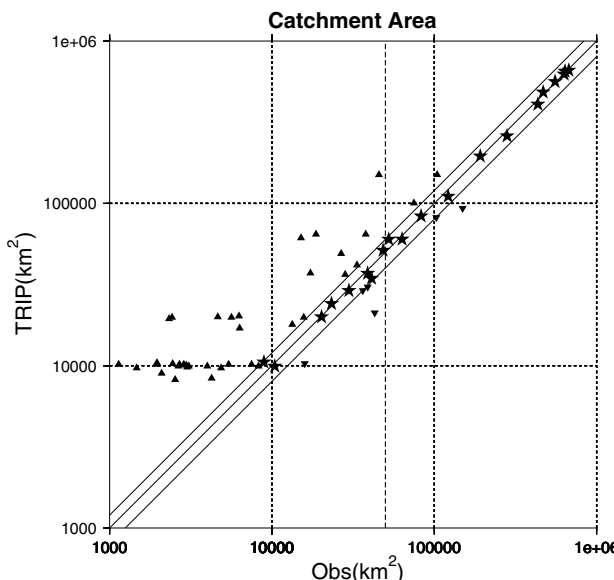


Figure 2 Observed and calculated catchment area for 69 reservoirs in USA. Observed catchment area information was obtained from WRD98. Star: error less than 20%, triangle: larger than 20% overestimation, inverse triangle: larger than 20% underestimation, dotted line: $50,000 \text{ km}^2$.

around 75% of that estimated by Baumgartner and Reichel (1975). Oki et al. (1999) attributed this to the fact that precipitation was underestimated in strong wind conditions, especially for snow. The underestimation of runoff is not a negligible problem, but the shift of discharge timing was the main focus of this study because the function of reservoirs is to control the timing of storage and release. For this reason, we judged that the no-reservoir simulation was appropriate for this study.

Global water withdrawal data

Global water withdrawal information was used to set monthly reservoir operating rules. Total water withdrawal was categorized as industrial, domestic, or irrigation. For industrial and domestic water withdrawal, we used gridded data from Oki et al. (2001), which consisted of global country-based industrial and domestic water withdrawal (WRI, 1998) at a $0.5^\circ \times 0.5^\circ$ spatial resolution. Monthly fluctuation was neglected for these sectors because the data did not exist.

For irrigation water withdrawal, we calculated global monthly values at the spatial resolution of TRIP following Döll and Siebert (2002), who estimated global irrigation water demand using CROPWAT (Smith, 1992), an irrigation water demand model with global gridded hydrometeorological data provided by New et al. (2000). To maintain consistent meteorological conditions in our simulation, we used the ISLSCP global meteorological dataset identical to that used in GSWP. See Appendices A and B for detailed descriptions of these calculations. Irrigation water withdrawal was specially treated for three reasons. First, irrigation water consumption comprises 85% of the annual global water consumption ($1753 \text{ m}^3 \text{ yr}^{-1}$ of $2074 \text{ m}^3 \text{ yr}^{-1}$ in 1995; Shiklomanov, 2000). Second, irrigation water is needed only during crop production, and therefore, has large seasonal variability. Third, irrigation is sensitive to meteorological conditions, which can be estimated using ISLSCP datasets.

Observed reservoir operation data

To validate the simulation results, we collected long-term observed storage, inflow, and release data for selected reservoirs. We collected monthly or daily operational records for 28 reservoirs with more than 10 yr of data (Table 1; Fig. 1). The data were distributed unequally, and were especially concentrated in the United States, where historical reservoir operation data are available from the world wide web. Thus, it should be noted that the validation was only conducted for a limited area of the world.

Model

We developed a new algorithm to set operating rules for individual reservoirs. A monthly time increment was adopted, and operating rules were determined in three steps. First, once each year, the annual total release for the following year was provisionally targeted to reproduce inter-annual fluctuations in release. Second, for each month, the release was provisionally targeted, accounting

for storage, inflow, and water demand along the lower reaches, to reproduce monthly fluctuations in release. Third, the targeted annual total and monthly releases were combined to determine each monthly release.

Inter-annual fluctuations in release

Operating rules were defined in relation to an "operational year," rather than a calendar year, and this was determined separately for each grid-square that contained a reservoir. First, each month was categorized as either a recharge month, where inflow exceeded the mean annual inflow, or a release month. Because we had only 2 yr of data, the mean annual discharge was sometimes affected by rainfall and drought extremes. We therefore tried to remove these effects by forcing consistency with respect to recharge months and release months. For example, if a release month occurred immediately after two continuous recharge months, and was immediately followed by two recharge months, the month was judged to have been affected by extreme events, and was altered to a recharge month, and vice versa. Thus, most grid-squares were assigned either to a release period, with contiguous release months, or to a recharge period, with contiguous recharge months. We defined the start of the operational year as the first month of a release period. In some arid areas, release and recharge periods can alternate more than once a year. In such cases, the first month of the release period immediately following the longest recharge period was taken as the start of the operational year.

Reservoir release has inter-annual fluctuations, reflecting those of inflow. We assumed that the annual total release for an operational year depended on the storage at the beginning of that operational year. If the initial storage was smaller than that for normal years, the release for the operating year was reduced to recover storage. If the storage was larger than normal, release was correspondingly increased, so that overflow was avoided which causes a sudden increase in outflow at the moment storage exceeds capacity. This was parameterized as follows. The total annual release for the y th operational year R_y ($\text{m}^3 \text{ yr}^{-1}$) was given as

$$R_y \approx k_{rls,y} \times I_{\text{mean}} \quad (2)$$

where $k_{rls,y}$ is the release coefficient for the y th operational year, and I_{mean} is the mean annual total inflow ($\text{m}^3 \text{ yr}^{-1}$). At the beginning of each operational year, $k_{rls,y}$ was calculated as

$$k_{rls,y} = S_{\text{first},y} / \alpha C \quad (3)$$

where $S_{\text{first},y}$ is the storage at the beginning of the y th operational year (which varies among years), α is a non-dimensional constant, and C is the total storage capacity of the reservoir. The constant α was set to 0.85 for all reservoirs. A sensitivity test was conducted for the constant α and is discussed in "Sensitivity test". Note that the storage capacity was assumed to correspond to that reported. In reality, the full storage capacity cannot be used because dead storage and surcharge storage are usually allocated. Thus, the simulated storage may be slightly overestimated.

Table 1 Validation sites

Name	Country	Completed	River at mouth	Capacity (10 ⁶ m ³)	Primary purpose ^A	Data type ^B	Data period ^C	Source
E.B.Campbell	Canada	1962	Nelson	2196	H	IO	1993–2002	a
Grand Rapids	Canada	1965	Nelson	9644	H	IO	1987–1996	b
Jenpeg	Canada	1975	Nelson	31790	CH	IO	1987–1997	b
Kelsey	Canada	1960	Nelson	1850	H	IO	1987–1998	b
Kettle Rapids	Canada	1970	Nelson	2529	H	IO	1987–1999	b
Missi Falls	Canada	1976	Nelson	28371	H	IO	1987–1997	b
Akosombo	Ghana	1965	Volta	150,000	H	SO	1965–1998	c
Bhumibol	Thailand	1964	Chao Phraya	13,462	IHC	SIO	1980–1996	d
Sirikit	Thailand	1974	Chao Phraya	9510	IHC	SIO	1980–1996	d
American Falls	USA	1978	Columbia	2062	IHR	SIO	1978–1995	e
Big Bend	USA	1963	Mississippi	2128	CHI	SIO	1971–2000	f
Buford	USA	1958	Apalachicola	2365	CHR	IO	1971–2000	g
Canyon Ferry	USA	1954	Mississippi	2402	HCI	SIO	1971–2000	h
Dworshak	USA	1973	Columbia	4278	CHR	IO	1974–1996	f
Flaming Gorge	USA	1964	Colorado	4674	SHR	SIO	1871–2000	i
Fort Peck	USA	1957	Mississippi	18,996	CHI	SIO	1971–2000	f
Fort Randall	USA	1954	Mississippi	4687	CHI	SIO	1971–2000	f
Garrison	USA	1953	Mississippi	22,820	CHI	SIO	1971–2000	f
Glen Canyon	USA	1964	Colorado	33,304	HIR	SIO	1971–2000	i
Grand Coulee	USA	1942	Columbia	11,795	ICH	SIO	1978–1990	f
Hungry Horse	USA	1953	Columbia	4278	IHC	SO	1971–2000	f
International Amistad	USA	1969	Rio Grande	4174	CIH	SIO	1977–2002	j
International Falcon	USA	1953	Rio Grande	3291	CIH	SIO	1971–2000	j
Libby	USA	1973	Columbia	7165	HCR	IO	1975–1990	f
Navajo	USA	1963	Colorado	2108	IRC	SIO	1971–2000	i
Oahe	USA	1966	Mississippi	23,806	CHI	SIO	1971–2000	f
Oroville	USA	1968	Sacramento	4364	SCI	SIO	1995–2004	k
Palisades	USA	1957	Columbia	1728	IHC	SI	1971–2000	e
Trinity	USA	1962	Klamath	3019	IHC	SIO	1971–2000	k
Yellowtail	USA	1966	Mississippi	1377	ICH	SIO	1971–2000	h

^a SaskPower (personal communication).^b Manitoba Hydro (personal communication).^c Andreini et al., 2000.^d Energy Generation Agency of Thailand (personal communication).^e US Bureau of Reclamation, Pacific Northwest Region.^f US Army Corps of Engineers, Northwest Division.^g US Army Corps of Engineers, South Atlantic Division.^h US Bureau of Reclamation, Great Plains Region.ⁱ US Bureau of Reclamation, Upper Colorado Region.^j International Border and Water Commission.^k California Department of Water Resources.

^A ‘‘H’’ for hydropower, ‘‘S’’ for water supply, ‘‘C’’ for flood control, ‘‘I’’ for irrigation water supply, ‘‘N’’ for navigation, ‘‘O’’ for others.

^B ‘‘S’’ for storage data, ‘‘I’’ for inflow data, ‘‘O’’ for outflow data.

^C We collected for 1971–2000 data. Some reservoir operator provides longer and/or later information.

Monthly fluctuations in release

Monthly release was set for each reservoir according to its primary purpose. WRD98 categorizes reservoir purpose into seven classes: hydropower, supply, flood control, irrigation, navigation, recreation, and other. We categorized reservoirs into two classes of purpose: irrigation and non-irrigation (i.e., all purposes other than irrigation). For an irrigation reservoir, monthly release was set in proportion to monthly irrigation, domestic, and industrial demand

downstream. Because we could not obtain monthly domestic and industrial demand, we assumed that they did not fluctuate inter-annually or seasonally; therefore, seasonal fluctuations were only caused by irrigation demand. For a non-irrigation reservoir, monthly release was set as constant throughout the year, except when the reservoir was expected to overflow or deplete the storage. We included flood control reservoirs in the non-irrigation category on the basis that the fundamental function of a flood control reservoir is to create flood control capacity in the high flow

season and constant release throughout the year reproduces this operation because it decreases reservoir storage during the low flow season.

For a non-irrigation reservoir, monthly release was parameterized as

$$r'_{m,y} = i_{\text{mean}} \quad (4)$$

where $r'_{m,y}$ is the provisional monthly release ($\text{m}^3 \text{s}^{-1}$), and i_{mean} is the mean annual inflow ($\text{m}^3 \text{s}^{-1}$).

For an irrigation reservoir, monthly release was parameterized as

$$r'_{m,y} = \begin{cases} \frac{i_{\text{mean}}}{2} \times \left(1 + \frac{\sum_{\text{area}} \{k_{\text{alc}} \times (d_{\text{irg},m,y} + d_{\text{ind}} + d_{\text{dom}})\}}{d_{\text{mean}}} \right), \\ (d_{\text{mean}} \geq 0.5 \times i_{\text{mean}}), \\ i_{\text{mean}} + \sum_{\text{area}} \{k_{\text{alc}} \times (d_{\text{irg},m,y} + d_{\text{ind}} + d_{\text{dom}})\} - d_{\text{mean}}, \\ (d_{\text{mean}} < 0.5 \times i_{\text{mean}}), \end{cases} \quad (5)$$

$$d_{\text{mean}} = \sum_{\text{area}} \{k_{\text{alc}} \times (d_{\text{irg},\text{mean}} + d_{\text{ind}} + d_{\text{dom}})\}, \quad (6)$$

where k_{alc} is an allocation coefficient for grid-squares that had more than one reservoir upstream; k_{alc} is proportional to the mean annual inflow from upstream reservoirs, and k_{alc} is 1 if the grid point has only one irrigation reservoir upstream; $d_{\text{irg},m,y}$ is the monthly irrigation water withdrawal ($\text{m}^3 \text{s}^{-1}$); d_{dom} is the domestic water withdrawal ($\text{m}^3 \text{s}^{-1}$); d_{ind} is the industrial water withdrawal ($\text{m}^3 \text{s}^{-1}$); and d_{mean} is the mean annual total water demand of the reservoir ($\text{m}^3 \text{s}^{-1}$). The subscripts m, y and mean indicate month, year and mean annual, respectively. The term \sum_{area} indicates integration over the basin downstream of each reservoir. Downstream was defined as including the reach down to the next reservoir, or, if there were no further reservoirs, down to the river mouth. We set the maximum distance as 10 grid intervals below the reservoir, approximately 1100 km downstream, or the distance traveled by released flow in a month (river flow velocity was set at 0.5 m s^{-1} or 1300 km mo^{-1}). Taking grid-square size ($1^\circ \times 1^\circ$ or $110 \times 110 \text{ km}$) into account, we summed the water withdrawals of the downstream grid-squares.

Three characteristics of Eq. (5) are now discussed. First, we set the minimum monthly release at 50% of the mean annual inflow. Irrigation water withdrawal exhibits large seasonal fluctuations and becomes zero during the non-cropping season. We examined reservoir operations for the 452 largest reservoirs in the world. These reservoirs tend to be located on the main branch or major tributary of a large basin; therefore, it is unrealistic to postulate months with no release. The observed mean monthly release from the reservoir operation data suggests that the maximum and minimum releases were, in most cases, within $\pm 50\%$. Second, we introduced both irrigation and domestic and industrial water withdrawal. The main issue is how to set release in non-crop months. Eq. (5) allows relatively larger release in a non-cropping month for basins with large domestic or industrial water demand. If irrigation water withdrawal is small, the operation approximates a non-irrigational operation (i.e., constant water withdrawal over the year). Third, two equations were used. The first was for reservoirs with large downstream water demand, with a monthly release set in relation to monthly fluctuations in

water demand. The second was for reservoirs with small downstream water demand, with monthly release set as equal to monthly water demand. In both cases, the minimum release is retained for each month.

The monthly release $r_{m,y}$ ($\text{m}^3 \text{s}^{-1}$) was calculated as

$$r_{m,y} = \begin{cases} k_{\text{rls},y} \times r'_{m,y}, & (c \geq 0.5), \\ \left(\frac{c}{0.5}\right)^2 k_{\text{rls},y} \times r'_{m,y} + \left\{1 - \left(\frac{c}{0.5}\right)^2\right\} i_{\text{m,y}}, & (0 \leq c < 0.5), \end{cases} \quad (7)$$

where c is the storage capacity to mean total annual inflow ratio ($c = C/I_{\text{mean}}$); and $k_{\text{rls},y}$ is the release coefficient (Eq. (3)), which reflects water storage at the beginning of the operational year; $r'_{m,y}$ is the provisional monthly release ($\text{m}^3 \text{s}^{-1}$; Eqs. (4) and (5)). Two equations were used. The first was for reservoirs with large storage capacity compared to annual inflow; release is independent of monthly inflow. The second was for reservoirs with small storage capacity compared to annual inflow. To avoid overflow and storage depletion during the year, release was influenced by monthly inflow. The squared exponent and criterion of 0.5 were set empirically. When c is zero, reservoir operation is identical to run-of-the-river flow. If storage exceeds storage capacity even when allocated water has been released, the excess volume of water is also released.

There are three fundamental advantages of this algorithm. First, it works with currently available data and is applicable to global river routing models. Second, release is constrained by mean annual inflow. Even if a biased inflow is supplied, the algorithm can flexibly generate release for the biased inflow. This is an essential feature in global river discharge simulations, which always contain some uncertainty and bias. Third, a release coefficient is used to buffer inter-annual fluctuations in inflow and stabilize release and storage simulations for more than 2 yr.

Sensitivity test

A sensitivity test was conducted for the constant α as follows. The monthly release and storage of the Glen Canyon Reservoir for the period 1980–1996 was simulated using the observed inflow and initial storage data (i.e., at 1 January 1980), using the water balance equation

$$S_{m,y} = S_{m-1,y} + (i_{m,y} - r_{m,y}) \cdot dt \quad (8)$$

where $S_{m,y}$ is the storage at the end of the month (m^3), $i_{m,y}$ is the inflow ($\text{m}^3 \text{s}^{-1}$), $r_{m,y}$ is the release ($\text{m}^3 \text{s}^{-1}$), and dt is time (s). The subscripts m and y indicate month and year, respectively. The primary purpose of the Glen Canyon Reservoir is hydropower generation, and $c > 0.5$ ($c = C/I_{\text{mean}} = 2.28$). Monthly release ($r_{m,y}$) was set as the mean annual inflow (annually constant). Five experiments were conducted with $\alpha = 0.65, 0.75, 0.85, 0.95$, and $k_{\text{rls}} = 1$ (Fig. 3). When α was changed from 0.65 to 0.95, the simulated storage increased proportionally for the whole simulation period. From 1989 to 1996, when annual inflow was close to the mean annual inflow, α showed low sensitivity to simulated release and high sensitivity to simulated storage. From 1983 to 1988, annual inflow was extremely high. The release coefficient was set high to produce large volume release, although storage was kept almost full. In this case, α had high sensitivity to simulated release (Eq. (3)) indicates that

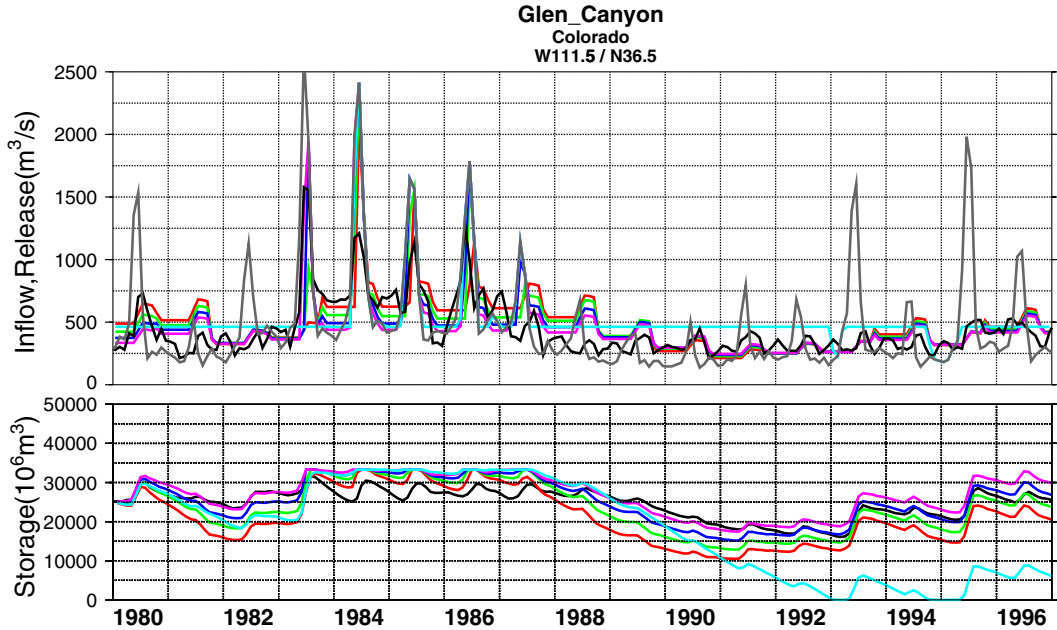


Figure 3 Sensitivity test for the constant α . Red, $\alpha = 0.65$; green, $\alpha = 0.75$; blue, $\alpha = 0.85$; pink, $\alpha = 0.95$; cyan, without the release coefficient (k_{rls}) or release constantly the mean annual inflow, black, observation; and Gray, inflow. (For interpretation of the references to colour in this figure legend, the reader is referred to the web version of this article.)

a smaller α produces a larger k_{rls}). At each value of α , the historical trend was reproduced, although the frequency of overflow increased with α . When k_{rls} was held constant at 1, storage significantly decreased in low flow periods (1988–1992) and storage attained a value of zero, which is quite unrealistic. The same experiment was conducted for other reservoirs and the results suggest that there is

an optimal α for each reservoir. For global application, α was set to 0.85.

Biased inflow is caused by overestimation of the catchment area and limitations of the global river discharge simulation. A sensitivity test for inflow bias was conducted using a similar method, using data for the Canyon Ferry Reservoir (hydropower, $c = C/I_{mean} = 0.48$). Five experiments

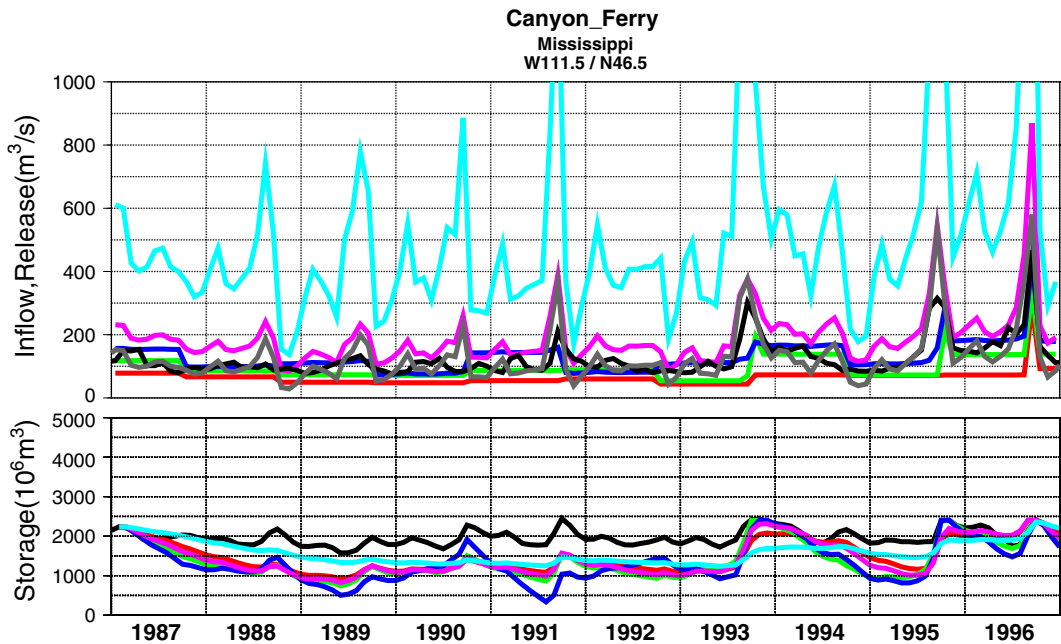


Figure 4 Sensitivity test for the biased inflow. Red, inflow was multiplied by 0.50; green, by 0.75; blue, by 1.00; pink, by 2.00; cyan, by 4.00; black, observation and gray: inflow. (For interpretation of the references to colour in this figure legend, the reader is referred to the web version of this article.)

were conducted multiplying inflow by 0.5, 0.75, 1.0, 2.0, and 4.0 (Fig. 4). When inflow was multiplied by 0.5 or 0.75, release decreased proportionally, and the annual change in storage also decreased. When inflow was multiplied by 2.0, release followed monthly fluctuations in inflow because c was 0.24 in this case, and the simulated storage was close to that at 0.5 and 0.75 of inflow. When inflow was multiplied by 4.0, c became 0.12. In this case, simulated storage showed little monthly fluctuation and reservoir release was close to run-of-the-river flow. The results suggest that even if inflow is strongly biased, the algorithm sets an operating rule that avoids overflow, which causes a sudden increase in outflow at the moment storage exceeds capacity, and the problem of storage depletion.

Simulation and analysis

We conducted both individual reservoir and global river discharge simulations. An individual reservoir simulation was conducted to check the performance of simulated reservoir operations. The monthly observed inflow and initial storage were input, and release and storage were simulated for reservoirs for which there was observed operation data. A global river discharge simulation was conducted to quantify the impact of reservoir operations on the terrestrial water cycle. This simulation included the operation of 452 individual reservoirs.

Individual reservoir simulation

The observed monthly inflow and initial storage were input to the model, and release and storage were calculated (Eq. (8)). Rainfall gain and evaporative loss, which are important water balance components, especially in reservoirs with large surface areas, were not accounted for in the current model. The mean annual inflow required to obtain $r_{m,y}$ was calculated from the whole observation period (Table 1). Five types of release were tested: non-irrigation, irrigation, constant, natural lake, and run-of-the-river. Non-irrigation and irrigation releases were described above. Constant release releases the mean annual inflow at a constant rate during the simulation period, except for two conditions, i.e., when storage is depleted and overflowed. Natural-lake release is Q_{out} (see Eq. (1)). Reservoir area was obtained from Lehner and Döll (2004). Storage (S) covers the range of $C - S_{max} \leq S \leq C$. Run-of-the-river release is identical to inflow; this release pattern is intended as a yardstick against which to compare the others.

Altogether, 28 simulations were conducted: 18 for non-irrigation and 10 for irrigation reservoirs (Table 1). For non-irrigation reservoirs, the simulation period was 10 yr (1987–1996) because most of the data covers this period. However, the E.B. Campbell Reservoir was simulated from 1993 to 2002, and the Oroville Reservoir from 1995 to 2004, owing to the restricted availability of data for these sites. Non-irrigation, constant, natural-lake, and run-of-the-river release were tested. For an irrigation reservoir, the simulation period was 2 yr (1987–1988), as covered by the ISLSCP dataset. Finally, the root mean square error (RMSE) was calculated for the simulated monthly release for each reservoir and each release type.

Global river discharge simulation

The reservoir operations scheme was coupled with TRIP, and a global river discharge simulation was conducted, accounting for reservoir operations ("reservoir simulation"). In this simulation, the global runoff field (before routing) was identical to that used in the no-reservoir simulation. The simulation period was 2 yr (1987–1988). The time steps for calculations were 12 h for routing and 1 month for applying the reservoir operating rule.

Simulation proceeded as follows. First, the operational year for each individual reservoir was calculated using the global river discharge field (after routing) derived from the no-reservoir simulation. Then, the initialization system commenced; the global runoff field for 1987 was iteratively input to the model until the initial river channel storage reached equilibrium. At this stage, reservoir operations were not considered. Next, the global runoff field for 1987 was iteratively input until the initial reservoir storage reached equilibrium, using reservoir operations. Next, the full simulation was conducted. The TRIP model was used to route runoff from each grid-square along the digital river network from the headwaters to the sea. In this procedure, if reservoirs were located in the relevant grid areas, the routing was changed from the standard channel flow scheme to the reservoir operations scheme. This procedure was applied to successive reservoirs progressing downstream, calculating the appropriate operating rule for each, and recording its hydrological state for each time step. For the first time step of an operational year, a reservoir operating rule was established for that year. Then, simulation results of river discharge and reservoir inflow, release, and storage were obtained at a 10-d resolution. In this way, individual reservoir operations were explicitly reflected in our global river discharge simulation. Finally, using the observed river discharge data provided by the Global River Discharge Center, the root mean square errors (RMSE) of the two global river simulation results were compared at 84 river gauging stations that had more than one reservoir in the upper reaches. The global simulation was based on the 2-yr global runoff field. The simulation results are affected by both the limited quality of the runoff field and the sample length of only 2 yr; these years may have been exceptionally wet, dry, or erratic.

In this model, we did not incorporate water extraction, which significantly affects river discharge in some basins, and is an important issue in global hydrological modeling. However, as Döll et al. (2003) noted, in many cases, simulated water withdrawal exceeds simulated river discharge for some period in a year. During this period, ground water or water from a surface reservoir may be used (Döll et al., 2003), and this water is not included in the current model. We concentrated on the difference between reservoir and no-reservoir simulations because we wanted to demonstrate only the changes in river flow produced by reservoir operations.

Impact assessment

We performed two analyses to examine the impact of reservoir operations on the global water cycle. First, we examined differences in the global monthly river discharge field

between reservoir and no-reservoir simulations to quantify monthly changes in river flow. Second, we examined river discharge and reservoir storage averaged at the continental scale. The world coastlines were divided into 18 sections (Table 2) following Dai and Trenberth (2002). Here, the tropical zone covered regions between 10°S and 10°N. We summed the discharge at river mouths for each section of coastline and obtained monthly river runoff. For each section, we examined the difference between the reservoir and no-reservoir simulations, the months of maximum increase and decrease, and the monthly reservoir storage.

Results and discussion

Individual reservoir simulations

For non-irrigation reservoirs, the RMSE of non-irrigation release was low for 11 of 18 reservoirs, and lower than, or equal to, that of run-of-the-river release at all reservoirs (Fig. 5). For irrigation reservoirs, the RMSE of irrigation release was low for 7 of 10 reservoirs; it was lower than, or equal to, that of run-of-the-river release at 8 reservoirs, but was larger at 2 reservoirs (Navajo Reservoir and Yellowtail Reservoir; Fig. 6). Irrigation release outperformed non-irrigation release at 7 of 10 reservoirs.

To show the capability and limitations of the simulations, we examined the best and worst results of release and storage: Glen Canyon Reservoir (non-irrigation reservoir; lowest RMSE compared to run-of-the-river release; Fig. 7), Oroville Reservoir (non-irrigation reservoir; RMSE similar to run-of-the-river release; Fig. 8), Sirikit Reservoir (irrigation reservoir; lowest RMSE compared to run-of-the-river release; Fig. 9), and Navajo Reservoir (irrigation reservoir; RMSE similar to run-of-the-river release; Fig. 10).

For the Glen Canyon Reservoir, the non-irrigation simulation reproduced the inter-annual trend in release, and consequently, in storage. In 1988 and 1989, release was overestimated, and thus, storage was underestimated. The underestimation of storage lasted 4 yr, but the discrepancy was gradually reduced. The constant release scheme resulted in overestimation in 1989–1995 (inflow was low in this period), and storage reached zero for some months in 1992–1995. Natural-lake release was similar to inflow. Storage fluctuated slightly and was almost always at capacity.

For the Oroville Reservoir, the non-irrigation simulation also roughly reproduced the inter-annual fluctuations in inflow; however, it showed significant error in both release and storage in 1997–1998 and 2000–2002. In both cases, the observed inflow and simulated release showed large discrepancies, which caused a significant change in storage (i.e., in 1998, 2000, and 2002, the simulated release was set at the minimum observed monthly inflow of the year, but in 1997 and 2001, it was set at the maximum monthly inflow of the year). Constant release resulted in overestimation from September 2000 to April 2001, and storage was set at almost zero for the whole of 2002. Natural-lake release and storage showed similar characteristics to those of the Glen Canyon Reservoir.

For the Sirikit reservoir, the irrigation simulation roughly reproduced the monthly trend of increasing or

decreasing release, although the magnitude was not accurate. Peaks in release were underestimated in March–April and overestimated in August–September. Natural-lake release followed fluctuations in inflow. Simulated storage was high during the simulation period, and monthly fluctuations were much smaller than those observed. The peaks in release in September 1987 and August 1988 were caused by overflow.

For the Navajo Reservoir, the irrigation simulation produced a peak in May–October, which is the estimated irrigation period for the lower reaches (the first peak, which appeared in May–June 1987, was caused by overflow). The observed operation shows almost constant flow, except during overflow.

The reservoir operations scheme produced the lowest RMSE at 18 of 28 reservoirs, and lower than, or equal to, run-of-the-river and natural-lake release at 25 of 28 reservoirs (Figs. 5 and 6). These results indicate that the reservoir operations scheme is a method for applying reservoir operations rules to global river routing models.

The non-irrigation release outperformed run-of-the-river release at every non-irrigation reservoir. Although in reality, every reservoir had seasonal fluctuations, the RMSE of non-irrigation release (calculated from monthly data) was dependent on the magnitude of the observed monthly fluctuations in release. In the case of the Glen Canyon Reservoir, the observed release had a clear seasonal pattern (high in January and July, low in April and October), but the difference between release for the maximum and minimum release months was relatively small ($\pm 22\%$, 30-yr monthly mean observations), and thus, the RMSE was small. To further decrease the RMSE, it would be necessary to reproduce the observed seasonal pattern of release. For example, the actual annual operation of the Oroville Reservoir in 1999 was described in a report by The State of California, Department of Water Resources (2004). In the flood control period (October–March), storage was held between the maximum and minimum flood control space. Release was high in July and August to meet water demands in the lower reaches, mainly for agriculture. This indicates a need for the additional parameters of flood control period, maximum flood control space, minimum flood control space, and irrigation water demand (the secondary purpose of the reservoir), to reproduce actual operations. We must consider problems with data availability and their expected effects, and carefully examine the opportunities for improvement that can be incorporated in relation to actual purpose-directed operations.

Introduction of the release coefficient (k_{rls}) reproduced the inter-annual release pattern. However, it only reflects storage at the beginning of an operational year, without accounting for inflow conditions. It sometimes allows significant changes in storage when release is much higher than inflow (e.g., this occurred for the Oroville Reservoir); this destabilizes the simulation. We may need to define a maximum monthly change in storage, although this would require a more complicated parameterization.

Irrigation release decreased the RMSE more than did non-irrigation release at 7 of 10 reservoirs. The total annual releases of irrigation and non-irrigation reservoirs are identical (Eq. (7)); the simulated monthly fluctuations estimated

Table 2 Impact of reservoir operation (result of reservoir simulation for 1987)

Section	Number of reservoirs	Total storage capacity (km ³)	Mean annual discharge (1000 m ³ s ⁻¹)	Maximum increase month				Maximum decrease month			
				Month	No-reservoir (1000 m ³ s ⁻¹)	Reservoir (1000 m ³ s ⁻¹)	Ratio (%)	Month	No-reservoir (1000 m ³ s ⁻¹)	Reservoir (1000 m ³ s ⁻¹)	Ratio (%)
Northeast Pacific	44	236.58	38.24	11	21.97	23.36	+6	4	19.02	15.99	-16
Southeast Pacific	1	1.00	7.81	5	11.95	12.04	+1	3	10.80	10.65	-1
Tropical east Pacific	5	15.34	10.63	3	2.63	2.96	+12	8	19.35	18.04	-7
Northwest Atlantic	101	797.54	89.08	12	57.26	63.59	+11	5	136.28	121.32	-11
Tropical west Atlantic	10	217.53	197.97	7	248.37	250.87	+1	1	140.28	136.74	-3
Southwest Atlantic	41	345.57	59.62	10	38.62	45.25	+17	4	83.07	74.34	-11
Northeast Atlantic	60	355.95	74.33	6	66.63	81.21	+22	1	76.75	67.25	-12
Tropical east Atlantic	12	193.07	62.50	2	37.44	39.17	+5	10	85.14	80.34	-6
Southeast Atlantic	5	15.29	1.38	8	0.61	0.81	+33	1	1.16	0.96	-18
West Indian	10	247.48	22.02	11	9.79	11.59	+18	5	37.18	34.10	-8
North Indian	34	194.42	46.66	1	10.62	12.83	+21	6	31.83	29.33	-8
East Indian	20	76.01	71.19	5	39.71	40.75	+3	12	63.30	61.89	-2
Northwest Pacific	50	491.09	99.00	2	35.76	39.10	+9	7	138.42	134.56	-3
Tropical west Pacific	0	0.00	69.19								
Southwest Pacific	11	35.28	10.83	2	10.79	11.40	+6	5	14.11	13.20	-6
West Arctic	1	74.30	11.96	4	0.06	0.65	+969	9	7.02	5.09	-27
East Arctic	17	511.87	63.71	4	2.52	6.88	+173	8	128.22	114.44	-11
Inland	30	318.21	35.56	8	41.82	55.12	+32	5	45.37	30.06	-34

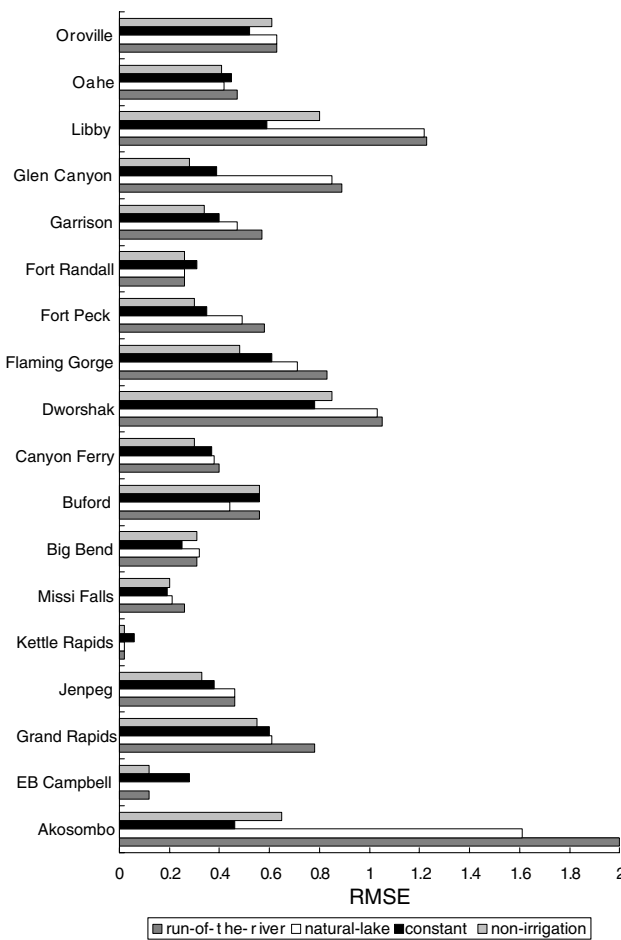


Figure 5 Root mean square error (RMSE) of individual reservoir simulation (non-irrigation reservoirs).

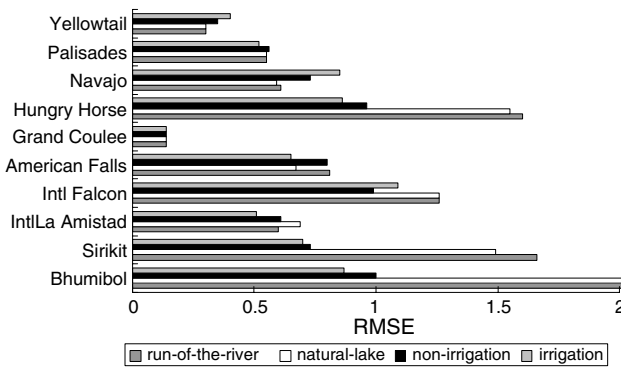


Figure 6 Root mean square error (RMSE) of individual reservoir simulation (irrigation reservoirs).

from irrigation water demand downstream contributed to decreased RMSE. There is a range of effects on RMSE among the reservoirs; RMSE decreased significantly from run-of-the-river release at Bhumibol, Sirikit, and Hungry Horse, and increased at International Falcon, Navajo, and Yellowtail. This was attributable to several causes: estimated irrigation water requirements or the crop calendar did not reflect actual irrigation; data on the meteorological forcing

was not accurate; and, reservoir operation may not have reflected irrigation demand for various reasons. However, even when the observed operations were not reproduced, a potential advantage of this approach is that release from a reservoir is synchronized with irrigation water demand in the simulation. If we add water intake to the model, the release from reservoirs compensates for river water that is removed for irrigation and other purposes. This type of reservoir operation may produce more realistic global water resources assessments (Vörösmarty et al., 2000; Oki et al., 2001; Alcamo et al., 2003).

The magnitudes of irrigation release were not well reproduced. To improve estimations, more detailed information on irrigation practices is needed. For example, at the Sirikit Reservoir, the magnitude of monthly release was overestimated in February–May and underestimated in June–November. In reality, the former is irrigation release for the dry season crop, which is dependent on the irrigation water supply, while the latter is irrigation release for the wet season crop, which is also fed by rain and increased river water flow. Reservoir water is not usually released in the wet season, except in extreme drought.

Natural-lake release was affected by the discrepancy between the actual inflow and the maximum outflow (Q_{out} , Eq. (1)). In the case of the Glen Canyon Reservoir, maximum release was calculated as $375 \text{ m}^3 \text{ s}^{-1}$, which is 81% of the mean annual inflow rate ($463 \text{ m}^3 \text{ s}^{-1}$). Therefore, the "active storage" was almost always full, and flows followed a run-of-the-river release pattern. A similar situation applied to other reservoirs. This explains why the natural-lake release had almost the same RMSE as did run-of-the-river release in many cases (Figs. 4 and 5). To apply this parameterization to reservoir operations, the maximum active storage depth (H) would have to be set in a different way. Another issue is that natural-lake release follows the seasonal pattern of inflow. Whether this assumption is valid should be considered in the future, after H has been more exactly defined.

The constant release pattern has a critical weakness in that it requires the same amount of release even in low flow years, and consequently, storage is reduced until it becomes zero. This destabilizes both release and storage in a long-term simulation.

Global reservoir simulations

The RMSEs of the results of reservoir and no-reservoir global simulations were compared at 84 river gauging stations that had more than one reservoir in the upper reaches (Fig. 11). The RMSE was decreased by more than 5% at 34 of 84 stations. Among the 34 stations, RMSE decreased by more than 20% at 15 stations. At 37 stations, the change in RMSE was below $\pm 5\%$ and was judged negligible. At 13 stations, RMSE increased by more than 5%. This suggests that application of the reservoir operations scheme is a method for incorporating reservoir operations within global river routing models. However, the results were derived from a 2-yr simulation, and this may not be a sufficient period from which to draw any strong conclusions.

The river discharge simulation results for the Colorado River (USA) at Above Little Colorado station below the Glen Canyon Reservoir are shown (Fig. 12). The reservoir simula-

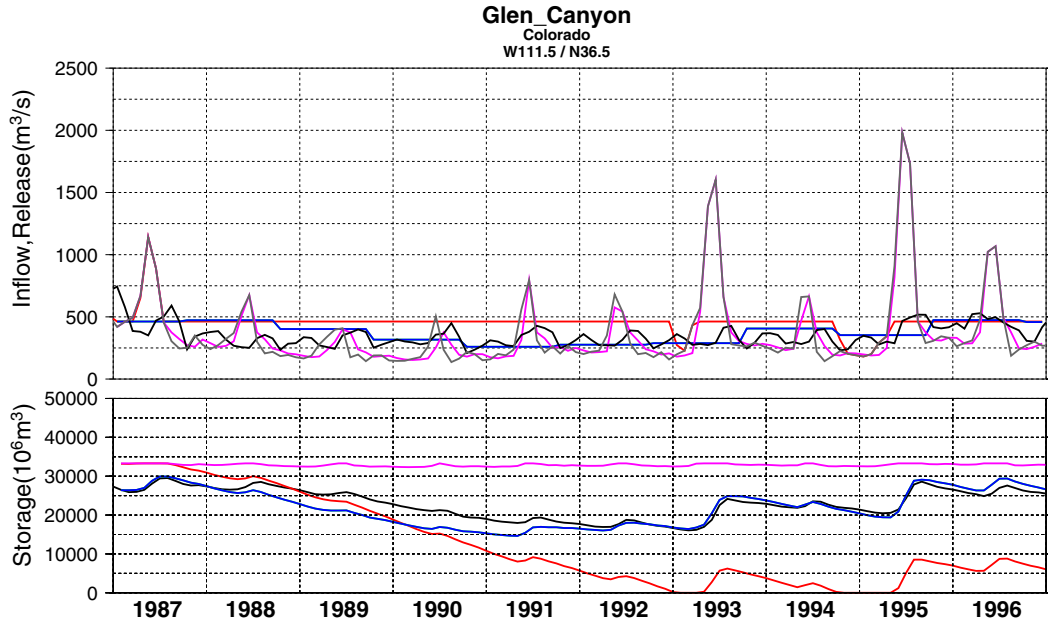


Figure 7 Individual reservoir simulation at the Glen Canyon Reservoir. The upper graph shows the inflow (gray) and release (pink: natural-lake release, red: constant release, blue: non-irrigation release, black: observation). The lower graph shows the storage of the reservoir. The color is the same as release. (For interpretation of the references to colour in this figure legend, the reader is referred to the web version of this article.)

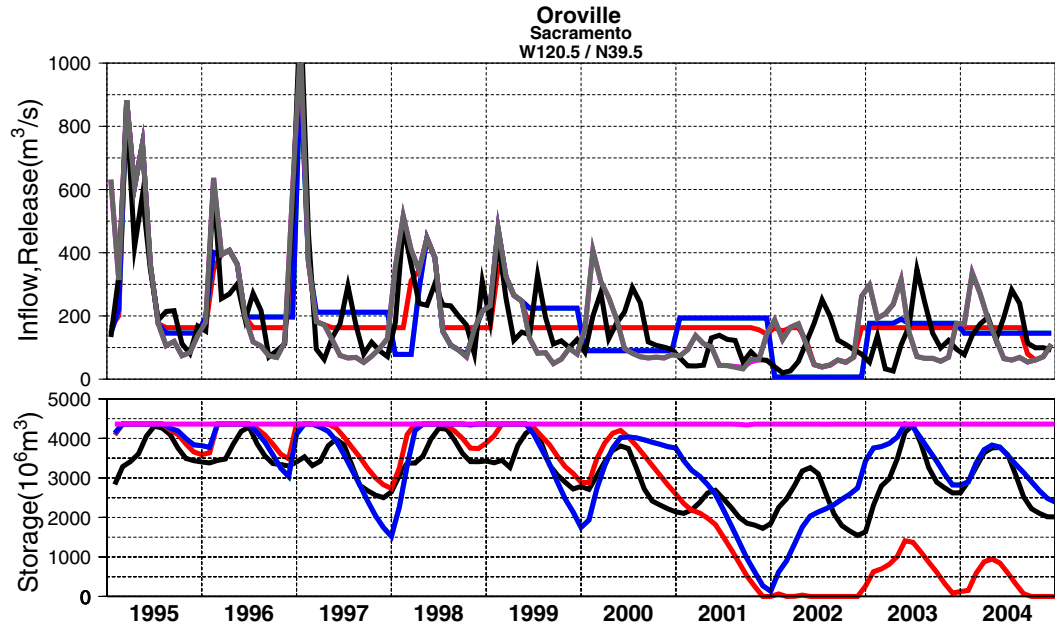


Figure 8 Individual reservoir simulation at the Oroville Reservoir. See Fig. 7 for legend.

tion reduced seasonal fluctuations in discharge, and the hydrograph became close to that observed. The no-reservoir simulation produced large fluctuations, with three peaks: March–May and August–September 1987 and April 1988. These did not correspond with actual conditions in the river. Both simulations showed consistent overestimation (no-reservoir, 35%; reservoir, 60%) that was caused by the biased input runoff data; in the reservoir simulation, the overestimation was further increased by the release of carry-over

storage. This indicates the simulation results may get worsened if the carry-over storage is not calculated accurately.

The river discharge simulation for the Chao Phraya River (Thailand) at Nakhon Sawan below the Bhumibol dam and the Sirikit dam are shown (Fig. 13). The reservoir simulation increased discharge in the low flow months (February–August) and decreased it in the remaining, high flow months. Although the change in February–August was limited, it improved the hydrograph. The observed data

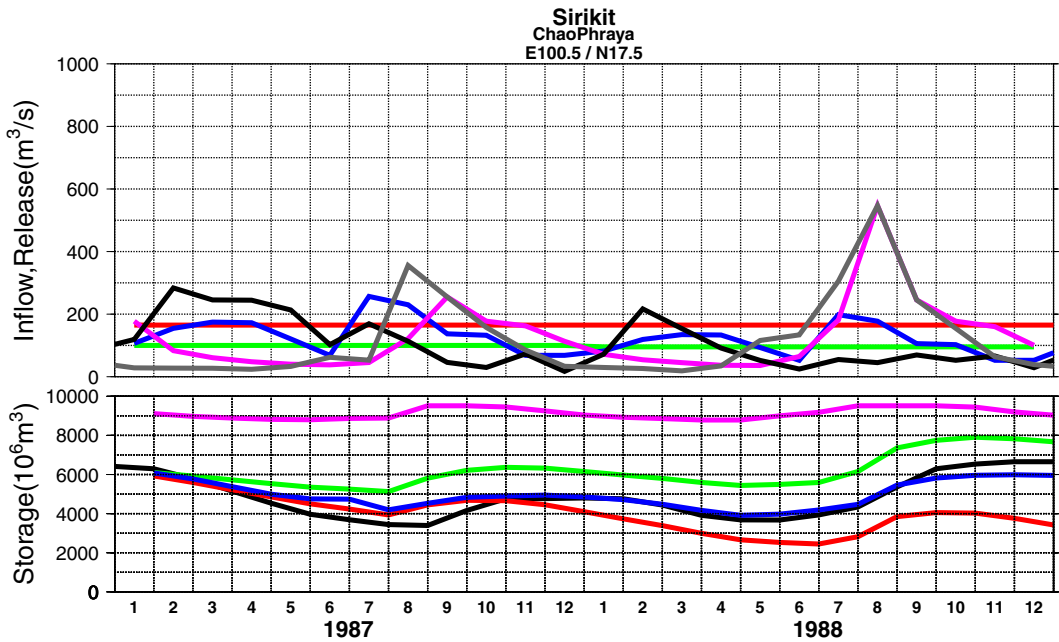


Figure 9 Individual reservoir simulation at the Sirikit Reservoir. The upper graph shows the inflow (gray) and release (pink: natural-lake release, red: constant release, blue: non-irrigation release, green: irrigation release, black: observation). The lower graph shows the storage of the reservoir. The color is the same as release. (For interpretation of the references to colour in this figure legend, the reader is referred to the web version of this article.)

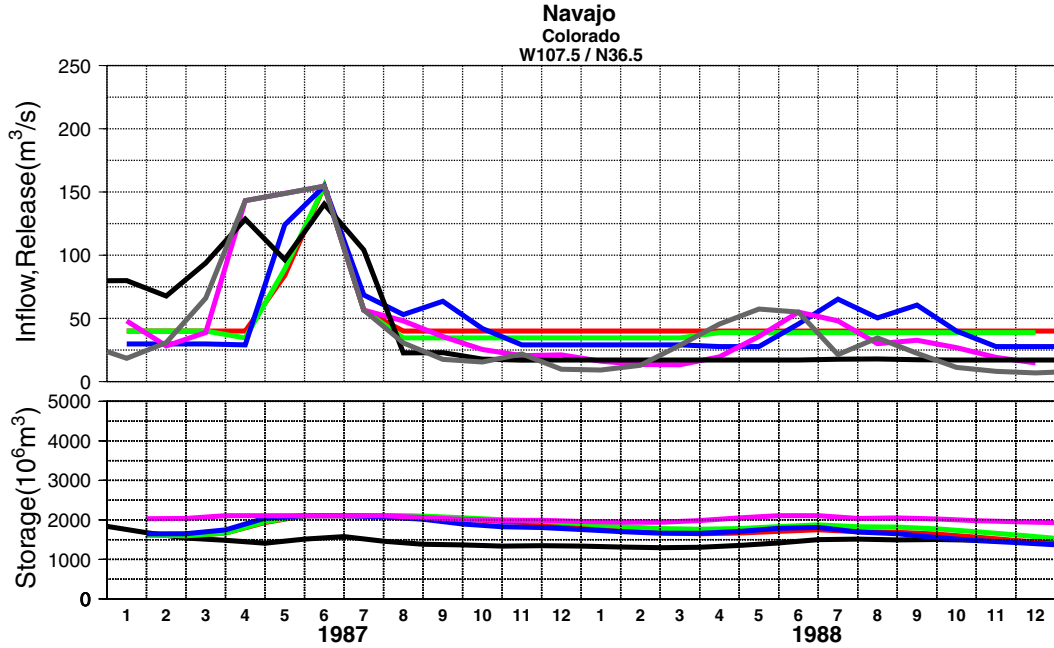


Figure 10 Individual reservoir simulation at the Navajo Reservoir. See Fig. 9 for legend.

showed two discharge peaks per year, in March and October. The no-reservoir simulation produced a peak only in October. At this station, the annual river discharge did not have a large bias (no-reservoir, +2%; reservoir -2%).

The simulated river discharge, and thus, the inflow to reservoirs, was affected by the limitations of the GSWP runoff dataset. Because the reservoir operations scheme used

mean annual inflow (average of a 2-yr simulation), release from the reservoir has the same bias as inflow. For the Colorado River, the simulation overestimated annual discharge by 35%. For the Chao Phraya River, there was small bias at the Nakhon Sawan river gauging station; however, at the Bhumibol Reservoir and the Sirikit Reservoir, discharges were underestimated considerably (Bhumibol: observed, $163 m^3 s^{-1}$; simulated, $95 m^3 s^{-1}$; Sirikit: observed,

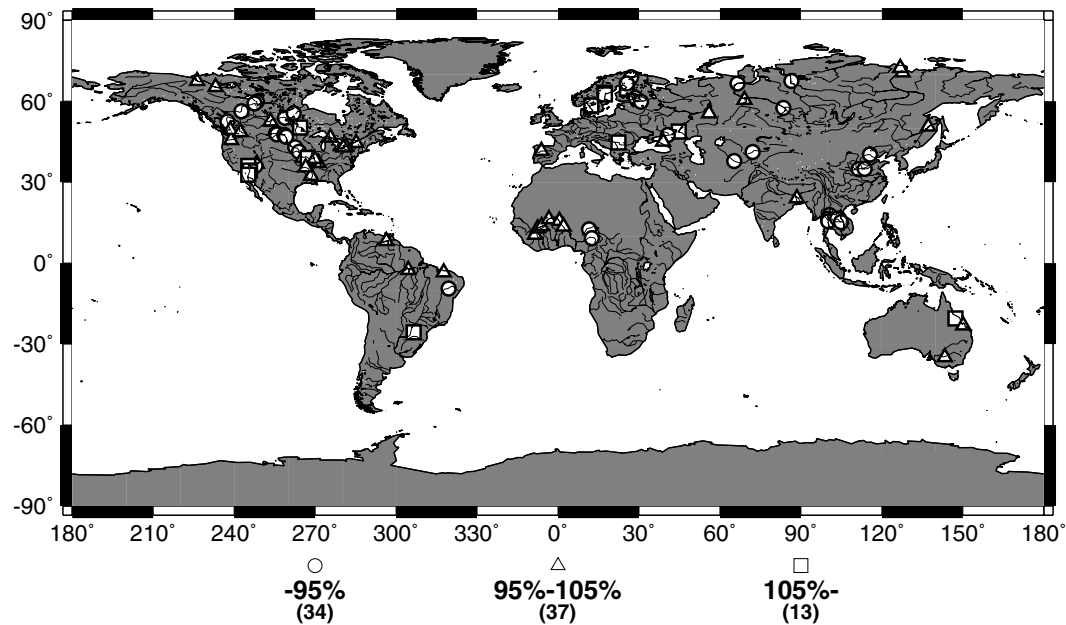


Figure 11 Change in root mean square error (RMSE) between reservoir simulation and no-reservoir simulation at 84 river gauging stations. Open circle: RMSE decreased more than 5%, open square: RMSE increased more than 5%, and open triangle: RMSE change was below 5%.

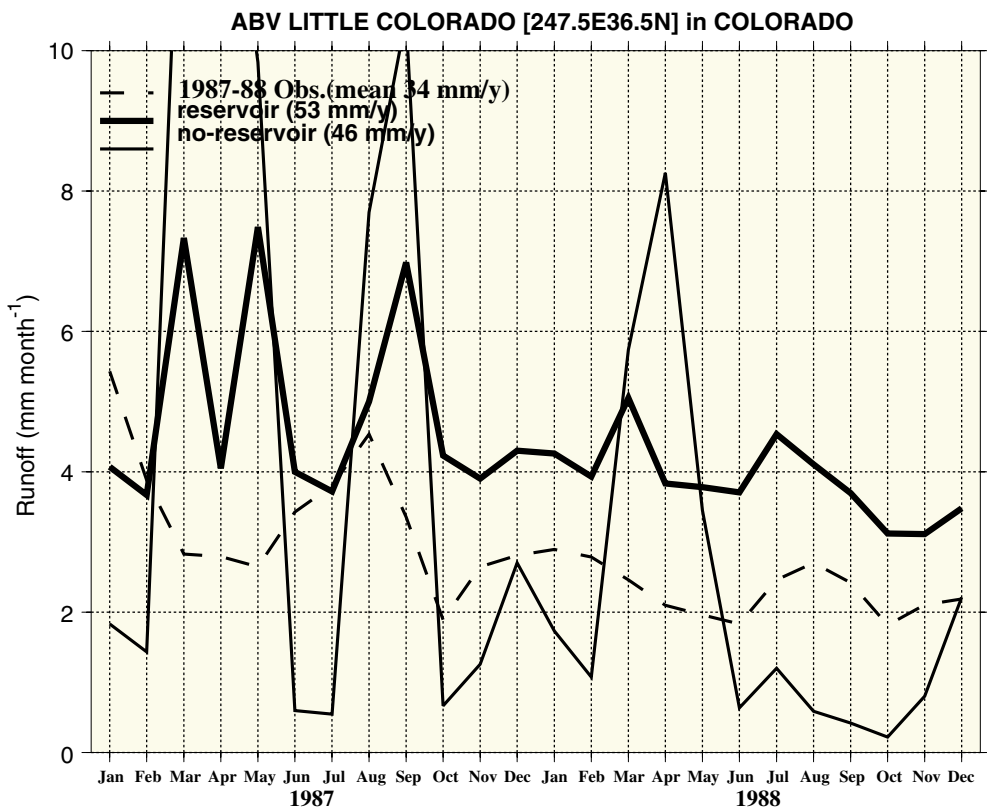


Figure 12 River discharge simulation result at the Above Little Colorado River gauging station in the Colorado River. Bold line, reservoir simulation; thin line, no-reservoir simulation; dotted line, observation.

$165 \text{ m}^3 \text{s}^{-1}$, simulated, $85 \text{ m}^3 \text{s}^{-1}$). The simulation underestimated the changes in river flow produced by reservoirs, i.e., if the runoff dataset were perfect, the two reservoirs would have released more in release months and saved more in

recharge months, and the hydrograph at Nakhon Sawan would have been closer to that observed using the same model. Reliable [global runoff datasets](#) are essential for improving simulations.

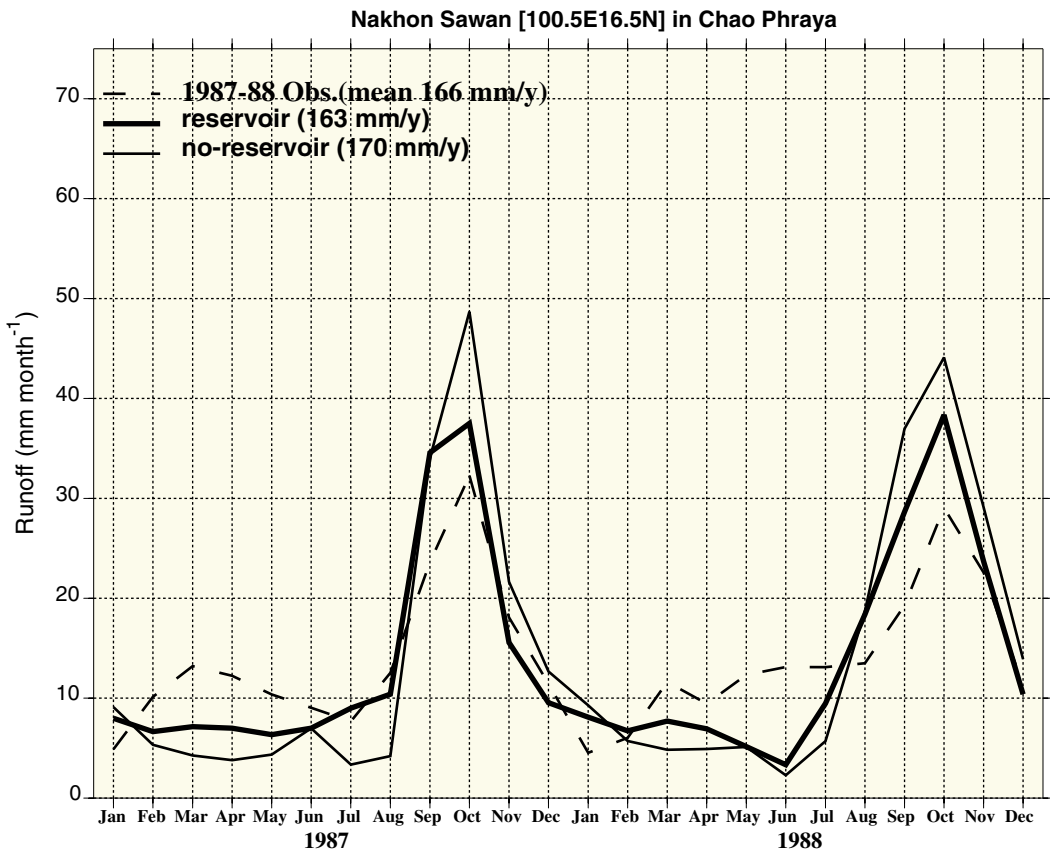


Figure 13 River discharge simulation results at the Nakhon Sawan gauging station in the Chao Phraya River. See Fig. 12 for legend.

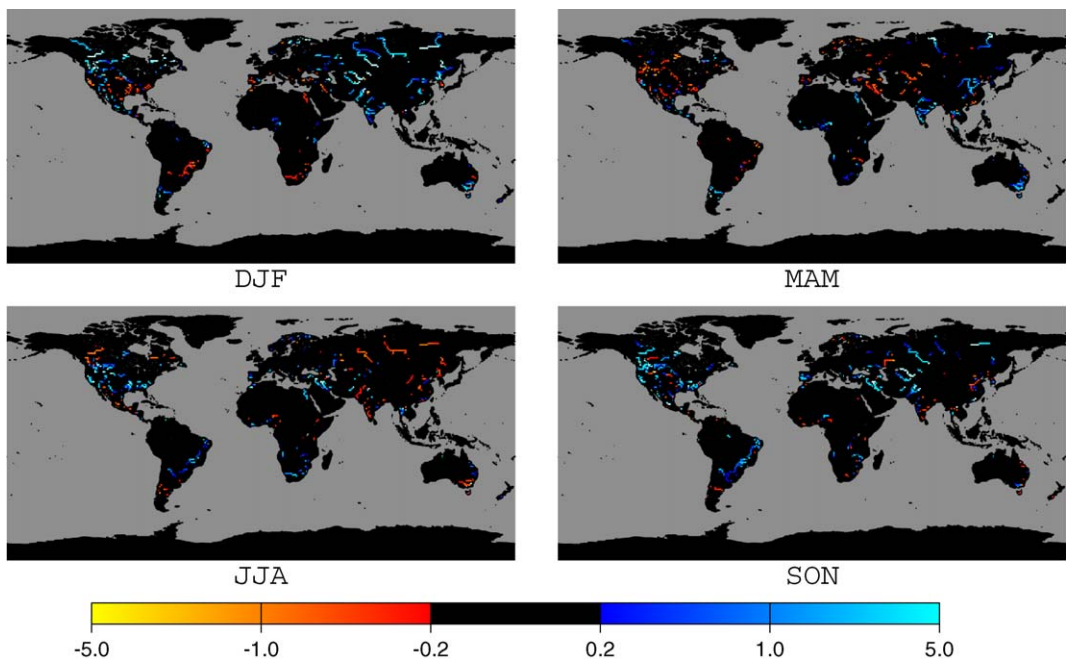


Figure 14 Normalized difference between reservoir simulation and no-reservoir simulation. Red, discharge is decreased by more than 20% owing to reservoir operation. Blue, discharge is increased by more than 20% owing to reservoir operation. DJF, December, January and February; MAM, March, April, May; JJA, June, July and August; SON, September, October and November.

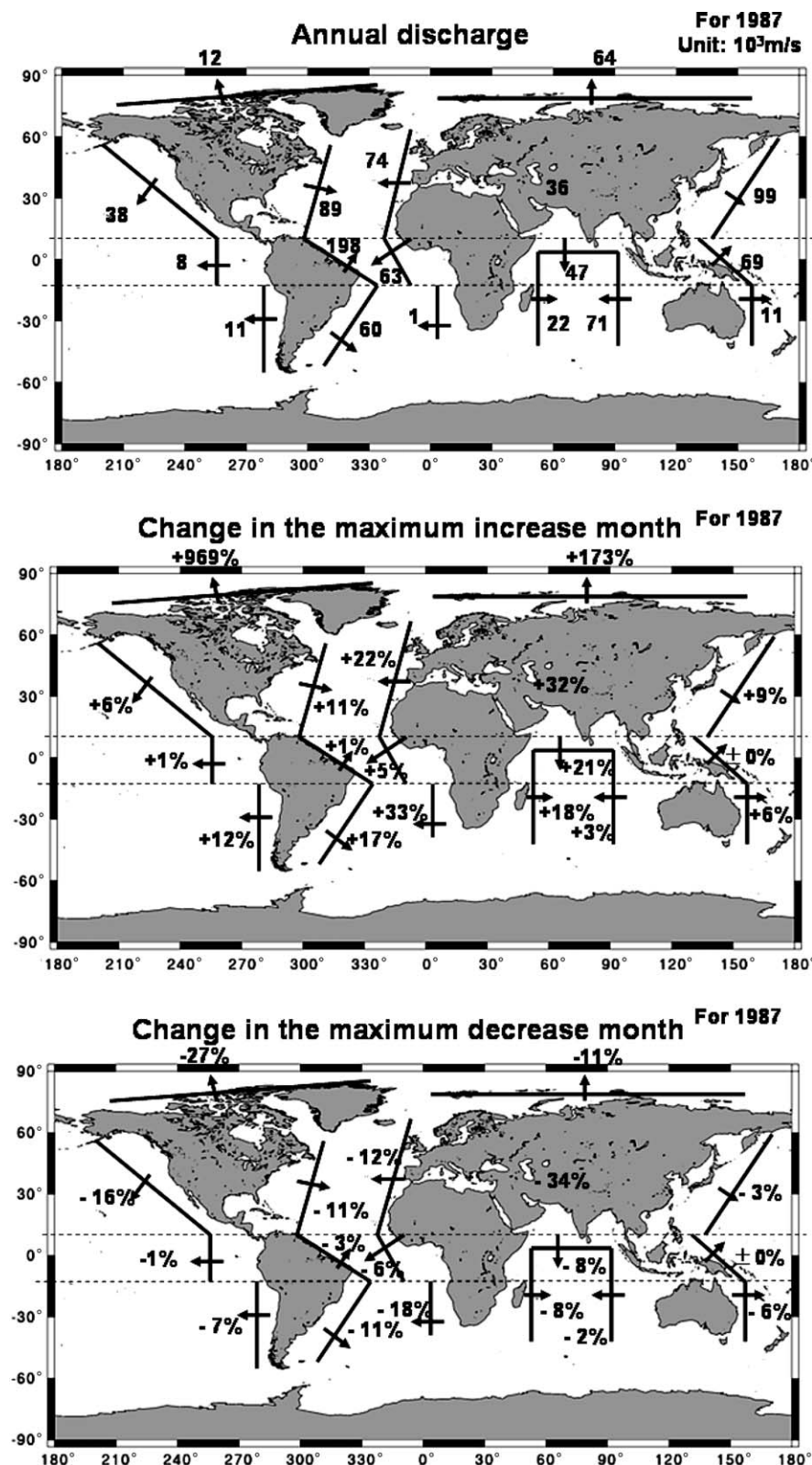


Figure 15 Impact of reservoir operation on terrestrial water cycle. The coastline of the world was divided into 17 sections following to Dai and Trenberth (2002). The top figure shows the annual mean discharge from each section. The middle and bottom figure shows the change in monthly river discharge between reservoir and no-reservoir simulation in the maximum increase month and the maximum decrease month. The number in the Eurasian continent indicates inland rivers.

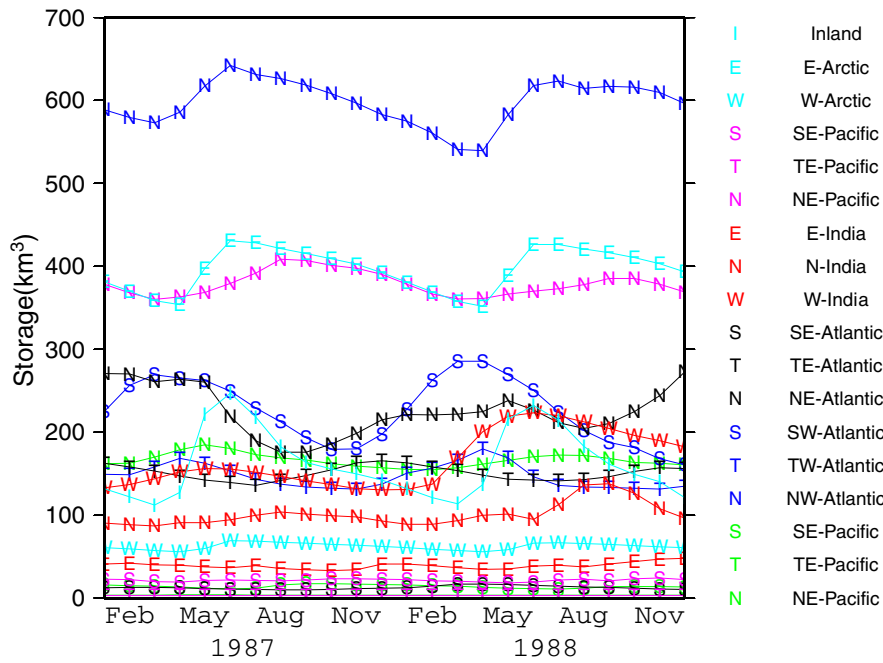


Figure 16 Monthly reservoir storage of reservoir simulation.

Impact assessment of reservoir operations

There were differences in the monthly discharge for no-reservoir and reservoir simulations (Fig. 14). Colored grids indicate that discharge was increased or decreased by more than 20% by reservoir operations. Because the impact only appears downstream of reservoirs, the affected areas appear as lines in Fig. 14; however, this represents the main flow of the world's largest rivers.

The discharges and changes in river flow for the 18 sections of coastline are shown in Table 2 and Fig. 15. For each section, the reservoir simulation increased discharge from 0% to 33% in the month of maximum increase (excluding the two Arctic Ocean sections) and decreased discharge from 0% to 34% for the month of maximum decrease. The active storage capacity for each section or the range between the maximum and minimum storage seldom exceeded one-third of total storage (Fig. 16).

Reservoir operations altered monthly discharge for individual basins by more than $\pm 20\%$. Most of the grids show blue color, indicating increased river discharge, which suggests that the dominant effect of reservoir operations was to increase river discharge in months of low flow. The effects of these changes in flow were still evident when combined for 18 regions of the world. There are limitations in the current simulation framework, but Figs. 14–16 show the potential impact of reservoir operations on the terrestrial water cycle. In the Northern hemisphere, the total number and storage capacity of reservoirs is large (Table 2), and reservoir operations increased discharge by more than 6% in the months of maximum increase. In contrast, in tropical areas, the difference in discharge was small because discharges were high and there were relatively few reservoirs.

The impact for the Arctic Ocean region was relatively large. Months of both maximum increase and decrease appeared in low flow seasons when land in the catchment

areas is frozen and little runoff is generated by LSMs. Huge reservoirs in Siberia, the primary purpose of which is hydro-power generation, release at a constant monthly rate and the water reaches the sea without freezing, even in winter. In the TRIP simulation, the freezing of river water or reservoir release was not considered, so the monthly release of water to the river, and its impact, was large.

The total global reservoir storage capacity is one-sixth of the annual global river discharge, although Fig. 16 suggests that the active storage for each region is quite limited. This is partly because storage and release tend to cancel each other out at the continental level; however, the results suggest that carry-over storage is far greater than active storage.

Conclusion

A reservoir operation scheme has been developed to establish reservoir operating rules for individual reservoirs in global river routing models. It works with currently available global data such as reservoir specifications, global runoff datasets, and water demand downstream. Incorporating the scheme with TRIP, a global river discharge simulation was conducted taking 452 individually operated reservoirs into account. The reservoir operation scheme improved reservoir release and river discharge simulations, as compared to earlier methods and to the run-of-the-river condition. Using the global river discharge simulation results, the impact of reservoir operation on the terrestrial water cycle was examined. The global simulation results indicated that the reservoir operation altered monthly discharge for individual basins substantially (more than $\pm 20\%$). Averaged over the continental scale, the maximum change in monthly river discharge varied from 0% to 34%, and the changes in reservoir storage were small as a proportion of the total storage capacity.

The reservoir operation scheme works with currently available global datasets. It fixes reservoir operations so that they are consistent with the runoff data; in addition, it is applicable to other global river routing models and runoff datasets. The global river discharge simulation, using the scheme quantitatively, showed that river discharge was altered by reservoir operations on a global basis. Additional work is underway with simulations, using runoff datasets from other published global runoff datasets to investigate the current uncertainty of the impact of reservoir operations among them. This framework can also provide a new approach to problems associated with assessing global water resources (Vörösmarty et al., 2000; Oki et al., 2001; Alcamo et al., 2003.). The water stored in reservoirs is an important component of water resources that are largely controllable by humans.

Finally, we address three limitations of the reservoir operation scheme. Firstly, the current scheme has a simple structure, designed to reproduce mainly inter-annual fluctuations in reservoir release, and monthly fluctuations estimated from irrigation water demand. This simplistic approach was shown to be largely valid but it inevitably produced errors because actual reservoir operation is more complex. For more sophisticated and realistic operation, more modules can be added; however, this will require access to additional global datasets. We need to consider data availability problems and their expected effects, and carefully examine the opportunities for improvement. Secondly, there is the problem of the limitation of the simulation periods covered. In this study, we conducted only a two-year simulation, which is too short to validate the capabilities of long-term simulation, or to discuss the long-term average impact of reservoir operations. We are optimistic that available global runoff datasets will be extended with respect to time periods, and improved with respect to accuracy, because of improvements to input meteorological data and modeling. The ongoing Second Global Soil Wetness Project (GSWP2) is expected to provide a breakthrough by providing daily output covering the state of the land surface over a period of 10 years; of particular importance will be the improved quality of the GSWP2 meteorological input data. Thirdly, owing to the limitations of long-term reservoir operation data, it is difficult to validate our model and simulation globally. As this study has shown, reservoirs have a large potential impact on the terrestrial water cycle, and it is essential that a global scheme be established for the systematic collection and storage of reservoir data.

Acknowledgements

The authors are grateful to Dr. Balazs Fekete and Dr. Bernhard Lehner for providing constructive comments and suggestions. The authors thank the Global Runoff Data Centre, the Energy Generation Agency of Thailand, GAME-T data center, US Bureau of Reclamation, US Army Corps of Engineers, California Department of Water Resources, International Border and Water Commission, SaskPower, Manitoba Hydro, and Professor Nick van de Giesen for providing their valuable data. This work was funded by the

Research Institute for Humanity and Nature and Core Research for Evolutional Science and Technology, Japan Science and Technology Agency.

Appendix A. Crop calendar estimation

A global monthly crop calendar was produced as follows. Döll and Siebert (2002) estimated a global daily crop calendar; their approach was to assign a score to the suitability for cropping of current hydrometeorological conditions, and find the maximum accumulated score, i.e., the best cropping times for points on a grid. The cropping period was assumed to be five months for every crop.

We have simplified their approach for monthly calculations. The suitability for cropping of the i th month is given by

$$m_{1,i} = \sum_{k=j}^{i+4} (b_k + a_k), \quad (\text{A.1})$$

where b_k is the basic score determined by monthly air temperature, and a_k is the additional score determined by monthly precipitation. In this study, the base score was set by considering monthly temperature at each grid square: 2 if the monthly mean temperature exceeded the mean annual, 1 if the monthly temperature exceeded the minimum temperature for cropping (5°C) and -99 if it was below the minimum temperature for cropping. An additional score was determined by taking monthly precipitation into account: 1 if monthly precipitation exceeded annual mean and 0 when it was below the annual mean. To avoid the situation where more than one month might have the best suitability score, $m_{1,i}$ was summed as

$$c_{1,i} = \sum_{k=i-1}^{i+1} m_{1,k} \quad (\text{A.2})$$

The month that had the highest c_1 was taken (provided it was greater than 0) as the first month of cropping.

Next, the potential for a double cropping area was determined:

$$m_{2,j} = \sum_{l=j}^{j+4} b_l \quad (\text{A.3})$$

$$c_{2,i,j} = m_{1,i} + m_{2,j} \quad (\text{A.4})$$

where the first term on the right side of Eq. (A.4) is the primary crop in the wet season and the second term is the secondary crop in the dry season. If $m_{1,i}$ and $m_{2,j}$ were both greater than 0, the grid square was judged to be a double cropping area. The maximum value of $c_{2,i,j}$ was found and i was taken as the first month of the primary crop, and j as that of the secondary crop. Note that i and j were set so that the primary crop season and the secondary crop season did not overlap.

Appendix B. Irrigation water demand estimation

Döll and Siebert (2002) estimated a global daily irrigation water demand using the CROPWAT method (Smith, 1992). Daily crop water demand (mm/day) is given by

$$d_{\text{CWD}} = k_c E_{\text{pot}} - P_{\text{eff}} \quad (\text{B.1})$$

where k_c is a non-dimensional crop coefficient reflecting variations in crop evapotranspiration as determined by crop growth rate. E_{pot} is the potential evapotranspiration (mm/day). P_{eff} is effective precipitation (mm/day), i.e., total precipitation less interception and surface runoff.

They distinguished only paddy and non-paddy cropping situations, because paddy fields are inundated and extra water is consumed. In this study we applied the paddy field approach to irrigated land in eastern India, South East Asian countries, southern China below Huai He, Korea, North Korea and Japan. The coefficient k_c was set for the first to fifth cropping months as: 0.4, 0.8, 1.0, 1.0, 0.8 for non-paddy and 0.1, 1.1, 1.1, 1.2 0.8 for paddy situations (Döll and Siebert, 2002).

Potential evapotranspiration was calculated using the FAO Penman-Monteith equation (Smith, 1992) and near-surface meteorological data of ISLSCP:

$$E_{\text{pot}} = \frac{0.408\Delta(R_n - G) + \gamma \frac{900}{T} U_2(e_a - e_d)}{\Delta + \gamma(1 + 0.34U_2)}, \quad (\text{B.2})$$

where R_n is the net radiation ($10^6 \text{ J m}^{-2} \text{ day}^{-1}$), G is the ground heat flux ($10^6 \text{ J m}^{-2} \text{ day}^{-1}$), T is the air temperature (K), U_2 is the wind speed 2 m above ground (m/s), e_a is the saturated vapor pressure (10^3 Pa), e_d is the vapor pressure (10^3 Pa), Δ is the rate of change of vapor pressure with temperature (10^3 Pa K), and γ is the psychometric constant ($0.067 \times 10^3 \text{ Pa K}^{-1}$).

Effective precipitation was calculated using the Soil Conservation Service Method given by the USDA (Smith, 1992):

$$P_{\text{eff}} = \begin{cases} P(1 - 0.048P), & P < 8.3, \\ 4.17 + 0.1P, & P \geq 8.3, \end{cases} \quad (\text{B.3})$$

where P is precipitation (mm/day).

Finally, irrigation water demand was obtained by multiplying crop water demand and irrigated area. Crop water demand for irrigation reservoirs is given by

$$q_{\text{dem}} = \frac{d_{\text{CWD}} \times k_{\text{area}} \times a}{k_{\text{eff}}} \quad (\text{B.4})$$

where two new non-dimensional coefficients are introduced. k_{area} is an area coefficient, the ratio of the area actually cultivated to that reported (some areas lie fallow). In this study we assumed $k_{\text{area}} = 1.0$ for the first cropping season, and $k_{\text{area}} = 0.3$ for the second cropping season. a is the irrigated area (km^2). Döll and Siebert (2000) produced a global map of irrigated areas that provides the global distribution of irrigated areas to $0.5^\circ \times 0.5^\circ$ spatial resolution. k_{eff} is irrigation efficiency, a non-dimensional coefficient that indicates the ratio of effectively used water to total intake water. The parameter k_{eff} was set to 0.5 globally; this may overestimate irrigation water demand in developed

countries, where k_{eff} is generally high, and underestimate it in developing countries.

The Global net annual irrigation water demand (with k_{eff} set to 1) and total annual irrigation water demand (k_{eff} set to 0.5) were calculated to be 1127 and 2254 km^3/year , respectively. This compares well with the result of Döll and Siebert (2002) of 1092 and 2549 km^3/year for 1961–1990 under average climatic conditions.

References

- Alcamo, J., Döll, P., Henrichs, T., Kaspar, F., Lehner, B., Rösh, T., Siebert, S., 2003. Development and testing of the WaterGAP2 global model of water use and availability. *Hydrological Sciences Journal* 48 (3), 317–338.
- Andreini, M., van de Giesen, N., van Edig, A., Fosu, M., Andah, W., 2000. Volta basin water balance. ZEF-Discussion papers on development policy 21, Bonn.
- Baumgartner, A., Reichel, E., 1975. The World Water Balance. Elsevier.
- Coe, M.T., 2000. Modeling terrestrial hydrological systems at the continental scale: testing the accuracy of an atmospheric GCM. *Journal of Climate* 13, 686–704.
- Dai, A., Trenberth, K.E., 2002. Estimates of freshwater discharge from continents: latitudinal and seasonal variations. *Journal of Hydrometeorology* 3, 660–687.
- Department of Water Resources, 2004. State of California, The resources agency, "State water project annual report of operations 1999".
- Dirmeyer, P.A., Dolman, A.J., Sato, N., 1999. The pilot phase of the global soil wetness project. *Bulletin of American Meteorological Society* 80, 851–878.
- Döll, P., Siebert, S., 2000. A digital global map of irrigated areas. *ICID Journal* 49 (2), 55–66.
- Döll, P., Siebert, S., 2002. Global modeling of irrigation water requirements. *Water Resources Research* 38-4, 1–10.
- Döll, P., Kasper, F., Lehner, B., 2003. A global hydrological model for deriving water availability indicators: model tuning and validation. *Journal of Hydrology* 270, 105–134.
- Dynesius, M., Nilsson, C., 1994. Fragmentation and flow regulation of river systems in the northern third of the world. *Science* 266, 753–762.
- Fekete, B.M., Vörösmarty, C.J., Grabs, W., 2000. Global composite runoff fields based on observed river discharge and simulated balances. Report 22, WMO GRDC.
- Haddeland, I., Lettenmaier, D.P., Skaugen, T. Effects of irrigation on the water and energy balances of the Colorado and Mekong river basins, *Journal of Hydrology* (in press).
- ICOLD, 1998. World Register of Dams. International Commission on Large Dams, Paris.
- Lehner, B., Döll, P., 2004. Development and validation of a global database of lakes, reservoirs and wetlands. *Journal of Hydrology* 296, 1–22.
- Meeson, B.W., Corprew, F.E., McManus, J.M.P., Myers, D.M., Closs, J.W., Sun, K.J., Sunday, D.J., Sellers, P.J., 1995. ISLSCP Initiative I – Global Datasets for Land–atmosphere Models. 1987–1988, NASA.
- Meigh, J.R., McKenzie, A.A., Sene, K.J., 1999. A grid-based approach to water scarcity estimates for eastern and southern Africa. *Water Resources Management* 13, 85–115.
- Miller, G., Russell, J.R., 1990. Global river runoff calculated from a global atmospheric general circulation model. *Journal of Hydrology* 117, 241–254.
- New, M., Hulme, M., Jones, P.D., 2000. Representing twentieth century spacetime climate variability, part II, Development of

- 1901–96 monthly grids of terrestrial surface climate. *Journal of Climate* 13, 2217–2238.
- Nilsson, C., Reidy, C.A., Dynesius, M., Revenga, C., 2005. Fragmentation and flow regulation of the world's large river systems. *Science* 308, 405–408.
- Oki, T., Sud, Y.C., 1998. Design of total runoff integrating pathways (TRIP) – a global river channel network. *Earth Interactions* 2. Available from: <<http://EarthInteractions.org>>.
- Oki, T., Nishimura, T., Dirmeyer, P., 1999. Assessment of annual runoff from land surface models using total runoff integrating pathways (TRIP). *Journal of the Meteorological Society of Japan B* 77-1, 235–255.
- Oki, T., Agata, Y., Kanae, S., Saruhashi, T., Yang, D., Musiake, K., 2001. Global assessment of current water resources using total runoff integrating pathways. *Hydrological Sciences Journal* 46-6, 983–995.
- Sellers, P.J., Mintz, Y., Sud, Y.C., Dalcher, A., 1986. A simple biosphere model (SiB) for use within general-circulation models. *Journal of Atmospheric Sciences* 43-6, 505–531.
- Shiklomanov, I.A., 2000. Appraisal and assessment of world water resources. *Water International* 25–1, 11–32.
- Shobunsha, 2000. Bertelsmann World Atlas (Japanese Edition), Shobunsha, Tokyo.
- Smith, M., 1992. CROPWAT – a computer program for irrigation planning and management.
- Vörösmarty, C.J., Sharma, K.P., Fekete, B.M., Copeland, A.H., Holden, J., Marble, J., Lough, J.A., 1997. The storage and aging of continental runoff in large reservoir systems of the world. *Ambio* 26 (4), 210–219.
- Vörösmarty, C.J., Green, P., Salisbury, J., Lammers, R.B., 2000. Global water resources: Vulnerability from climate change and population growth. *Science* 289, 284–288.
- WCD, 2000. Dams and development: A framework for decision-making, The World Commission on Dams.
- WRI, 1998. 1998–99 World resources. Report of UNEP, UNDP & World Bank. Oxford University Press, Oxford, UK.